Advances in Science and Technology Research Journal

Advances in Science and Technology Research Journal 2023, 17(1), 252–266
https://doi.org/10.12913/22998624/158029
ISSN 2299-8624, License CC-BY 4.0

Received: 2022.12.05
Accepted: 2023.01.17
Published: 2023.02.01

A Comparison of Two-Roll and Three-Roll Cross Wedge Rolling Processes

Zbigniew Pater[1*]

[1] Lublin University of Technology, ul. Nadbystrzycka 36, 20-618 Lublin, Poland
e-mail: z.pater@pollub.pl

ABSTRACT

Cross wedge rolling (CWR) is used for producing stepped axles and shafts as well as die forging preforms. In current industrial practice, CWR conducted with two tools is predominantly used, with the wedges mounted on rolls or flat tool plates. However, CWR can also be performed with the use of three wedge rolls. This paper begins with a review of previous studies on CWR conducted with the use of three rolls. After that, numerical simulations of two- and three-roll CWR processes for the same shaft are described. Obtained numerical results are then used to compare the two processes in terms of material flow kinematics, material temperature, stresses and strains, failure modes, as well as load and energy parameters. Finally, the Conclusions section presents the advantages of three-roll cross wedge rolling, providing a good starting point for further research on this promising forming method.

Keywords: cross wedge rolling, FEM, tools, load, energy.

INTRODUCTION

Shafts and stepped axles are widely used in mechanical engineering. Components of this type are formed from semi-finished products manufactured by forging or, more rarely, cross wedge rolling (CWR) [1]. The latter manufacturing method, which is becoming more and more popular, is particularly interesting in this context. The predominant failure mode in CWR is the formation of internal cracks in the axial zone of the workpiece [2]. The risk of crack formation can however be considerably reduced when the CWR process is conducted with the use of three, rather than two, rolls [3]. Given this fact, for this study it was of interest to investigate the possibilities offered by three-roll cross wedge rolling.

A three-roll rolling process for manufacturing axles was developed already in 1892 by Slick [4], who proposed the use of tools with eccentric working surfaces. The design also included the method for automatic (gravitational) loading the blank and ejecting the finished product without stopping rotation of the rolls. In light of today's knowledge however, the tools proposed by Slick were unsuitable for the manufacture of axles. More suited for the purpose were the tools developed by Schneider in 1901 [5]. The design assumed that axles would be manufactured in two operations. In the first operation, three rolls provided with helically-wound guides would be used for deforming the central portion of the shaft. In the other operation, a separate set of tools provided with annular guides would be used for shaping the journal portions of the axle. The solutions could not however be tested due to a lack of machines (roll mills). The first three-roll machine for rolling stepped shafts was patented by Wurster in 1924 [6]. The machine was a hydraulic press with two rolls mounted on the table. The two rolls were rotated by an electric engine. The third roll was mounted in the press slide and pressed by the slide to the other two rolls. Importantly, however, the third roll was not electrically driven but rotated due to friction forces. A rotary forging machine with three mechanically driven rolls was patented by Brown in 1944 [7]. The machine was intended for shaping bullets from cylindrical bars. Another machine for rolling stepped shafts was patented by Wilson in 1954 [8]. With

this machine, the workpiece was deformed by means of three roll-dies with ridges eccentrically mounted on the rolls, with their width increasing as the tools cut into the billet. This type of rolling was called as ramp rolling, as opposed to wedge rolling wherein wedge tools were used. Rogers [9] demonstrated that ramp rolling could be used for manufacturing parts with their lengths of up to four times the billet diameter value, whereas in wedge rolling this length could be up to ten times the billet diameter. Promising experimental results in this area led Redman Engineering to construct prototypes of three-roll mills that were tested at British plants for manufacturing drop forging preforms [10]. Designed in two versions, the machines could be used for forming parts with their diameters of up to 50 mm and lengths of up to 300 mm. Detailed experiments on three-roll rolling were conducted at Toyota Central Research & Development Laboratories, Inc. [11]. Obtained experimental results confirmed that the process was an effective method for rolling parts with a cross-sectional reduction of up to 70%. For practical application, it was recommended using wedge tools with a forming angle of $\alpha = 15 \div 20°$ and a spreading angle of $\beta<15°$.

The development of numerical methods opened up new possibilities for conducting research on three-roll CWR. The use of FEM made it possible to investigate the potential of this rolling method for manufacturing hollow parts. The first simulation ever in this respect was performed by Pater et al. [12], who found that the use of three rolls resulted in quick removal of cross-sectional defects. Bartnicki & Pater [13] investigated three-roll CWR conducted with variable tool parameters and identified failure modes in this process, such as slipping and cross-sectional triangulation. Pater [14] used FEM to determine stresses and strains in a solid workpiece that was deformed with the use of three rolls. The distribution of temperature in a part rolled with the use of three rolls was analysed by Qiu et al. [15]. A concept of a three-roll CWR process for manufacturing hollow rail axles was presented by Pater et al. [16]. In this process the workpiece was deformed into the desired shape during two revolutions of three coupled rolls. Three-roll CWR also became a basis for developing new methods for manufacturing hollow parts, including cross wedge rolling by means of one flat wedge and two shaped rolls [17], rotary compression with the use of rolls [18, 19], and three-roll rolling with eccentrically mounted tool segments [20].

It is assumed that the stress state in a rolling process conducted with three tools differs from that performed using two rolls. Nevertheless, there are no studies to confirm that assumption. In this respect one may, to some extent, draw upon results obtained from previous studies on skew rolling. Pater et al. [21] compared tube piercing processes conducted in two- and three-roll mills. The comparison revealed that the three-roll process was less energy-consuming and thus more advantageous. Skripalenko et al. [22] found that in two-roll CWR material fracture occurred along the axis of the workpiece, whereas in three-roll CWR the cracks were ring-shaped. This finding was confirmed by Yamane et al. [23]. Pater et al. [24] used FEM to compare the stress states in two- and three-roll skew rolling processes. Obtained results showed significant differences in the Lode angle parameter describing shear stresses in the forming process.

In light of the above literature review, there is a clear justification and necessity to conduct research on CWR performed with the use of three rolls. It has been a very long time since this process was last investigated. Although previous studies signalled that three-roll CWR offered numerous advantages, two-roll CWR has become dominant in industrial practice. For this study, numerical results of CWR processes for manufacturing the same part with the use of three and two rolls are compared. Obtained results are presented in this paper.

SCOPE OF THE ANALYSIS

This study investigates a CWR process for a stepped shaft that is shown in Figure 1. This component is manufactured from a cylindrical billet with a diameter of 40 mm, this value being at the same time the diameter value of the steps on the shaft ends that were not deformed. In its central region, the shaft had two steps with two different diameters of 25 and 35 mm. The steps were rolled with a reduction ratio δ (expressed as a ratio of the billet diameter d_0 to the diameter d of a rolled step, and used for describing strain in CWR) of 1.6 and 1.143, respectively.

Figures 2 and 3 show the wedge tools used in two- and three-roll CWR, respectively. For both cases, the working part of the tool (wedge)

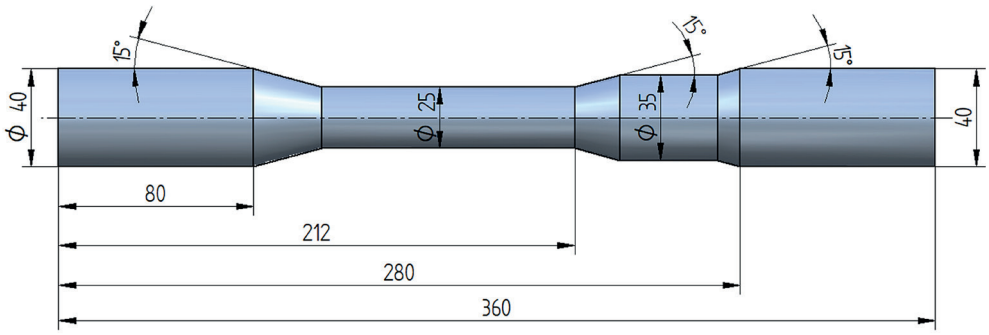

Fig. 1. Stepped shaft used for comparative analysis

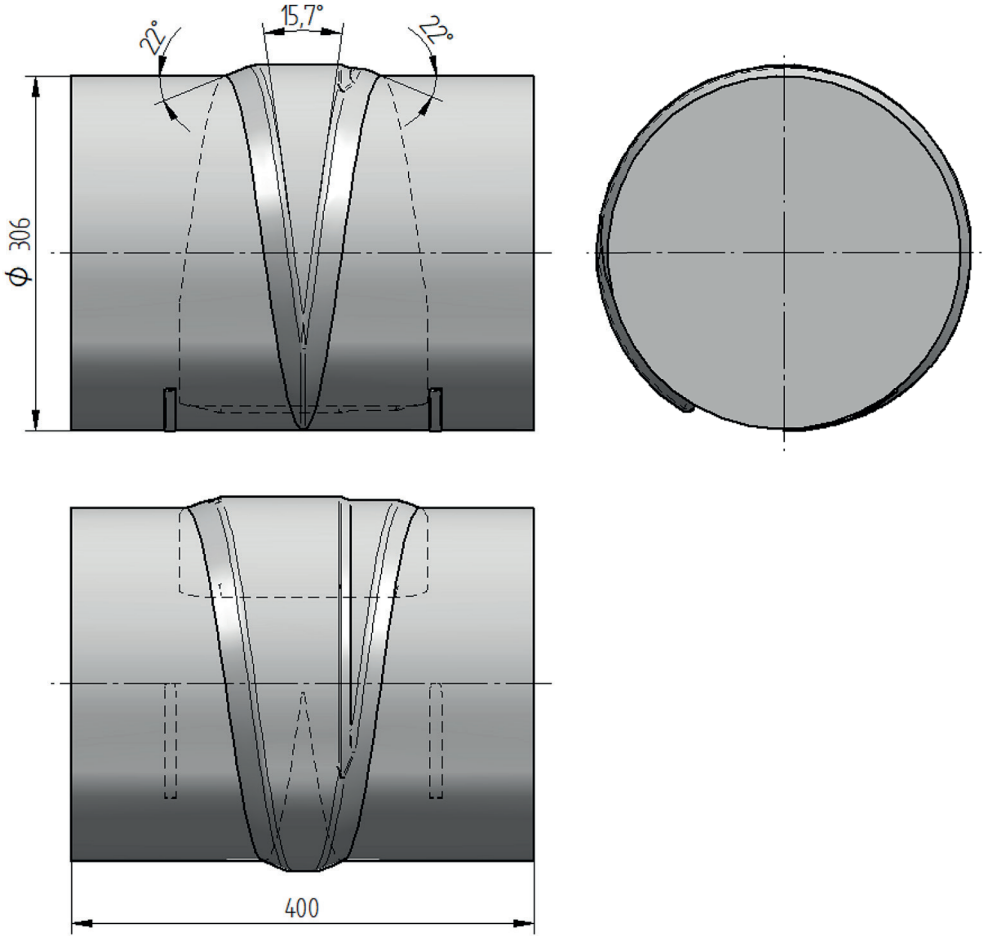

Fig. 2. Wedge tool used in two-roll CWR

was wound up over a 11/12 of the circumference of the rolls and described by a forming angle of α = 22°. In two-roll CWR the distance between the axis of the rolls and the workpiece was set to 200 mm, while in three-roll CWR the distance was smaller and set to 90.5 mm (the interaxial distance was reduced in order to satisfy the no-contact condition between the mating tools, according to which the limit value of this parameter was 7.464 of the radius of the rolled step). The differences in the diameter of the rolls resulted in different values of the spreading angle β, these values being 7.85° and 14.35° for two-roll CWR and three-roll CWR, respectively.

The two investigated CWR processes were compared via numerical simulations. The simulations were performed using the FEM-based simulation software Simufact.Forming. The software had been used in many previous studies for comparing cross and skew rolling processes [25–36], and obtained numerical results showed high agreement with experimental findings.

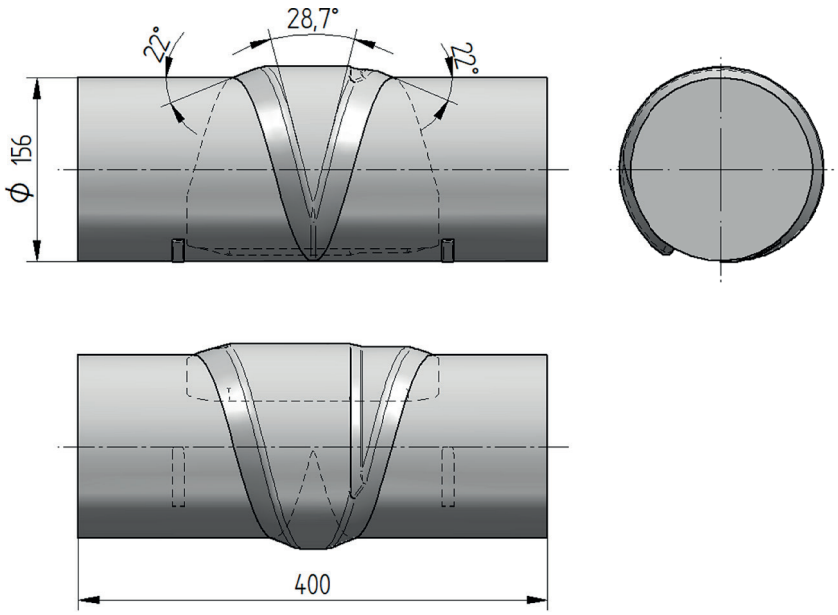

Fig. 3. Wedge tool used in three-roll CWR

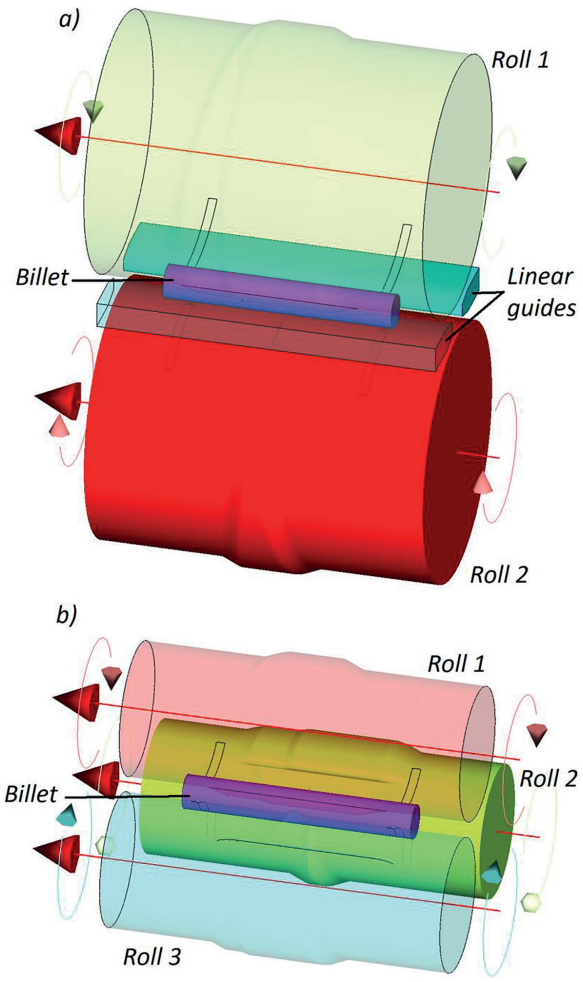

Fig. 4. Geometrical models of the numerically analysed CWR processes: a) two-roll CWR, b) three-roll CWR

Figure 4 shows the geometrical models of the two analysed CWR processes designed in Simufact.Forming. The model of two-roll CWR consisted of a billet and rolls as well as two guides for keeping the workpiece in the forming zone. All tools were assumed to be ideally rigid bodies, while the workpiece was assigned the properties of an elastic-plastic body. The billet was assigned the properties of 42CrMo4 steel, the material model of which was obtained from the material database library of the employed computer software.

The workpiece was modelled using hexahedral finite elements. Automatic remeshing took place when the strain increase in any node exceeded a value of 0.4. Figure 5 shows the division of the workpiece into finite elements at the beginning and toward the end of the rolling process.

The tools were rotated with the same constant speed of 10 rev/min in both analysed CWR processes. Contact conditions between the workpiece and the tools were described by the Tresca friction model, with the friction factor set to 1 for the rolls and to 0.4 for the guides. Thermal phenomena occurring during CWR were taken into consideration. The temperature of the billet was set to 1150 °C, the temperature of all tools was maintained constant at 200 °C during the forming process, and the coefficient of heat transfer between the tools and the workpiece was set to 10 kW/m^{2}K.

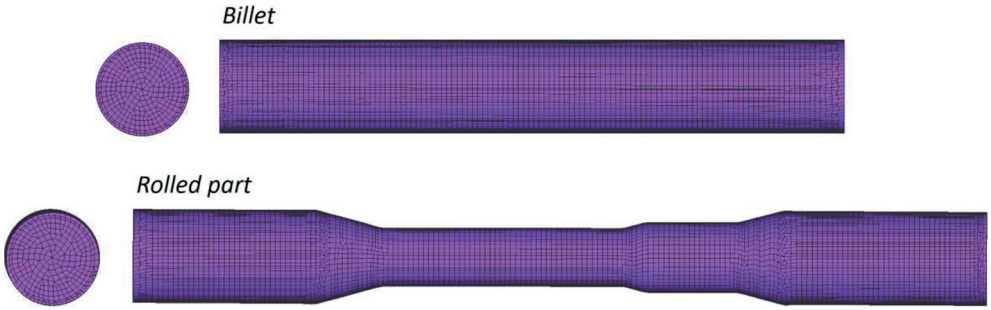

Fig. 5. Workpiece discretization employed in numerical analysis

RESULTS

Material flow kinematics

Given the assumption of the same rotational speed of the tools, it was possible to make a direct comparison between the two- and three-roll CWR processes for manufacturing a stepped shaft. Fig. 6 shows the changes in the shape of the workpiece for both analysed CWR processes. The forming stage starts when the wedges cut into the centre of the billet. The cross-sectional reduction initiated in this region is then developed toward the ends of the workpiece. The final stage consists of sizing in which all cross-sectional defects are ultimately removed. It must be stressed that the required shape of the stepped shaft (see Fig. 1) was achieved in both CWR processes and that no failure modes occurred in either of the processes.

Figure 7 shows the changes in the location of the measuring points that were initially distributed in a radial manner, i.e. along the line crossing the centre of the workpiece. As a result of the forming process, the line (which was initially straight) was bent into an S letter shape (cross-sectional view), which can be explained by variations in the circumferential metal flow. At the same time, however, the front view reveals that the line is bent in the opposite direction to that of the wedge (which moves sideways). This is caused by the friction forces on the contact surface as they impede the material's flow in the longitudinal direction. The number of the rolls used in CWR has an insignificant effect on the shape of the line. It can however be observed that for three-roll CWR, the surface flow of the material in the longitudinal direction is impeded to a greater extent.

The greatest differences in material flow kinematics can be observed in the cross-sectional

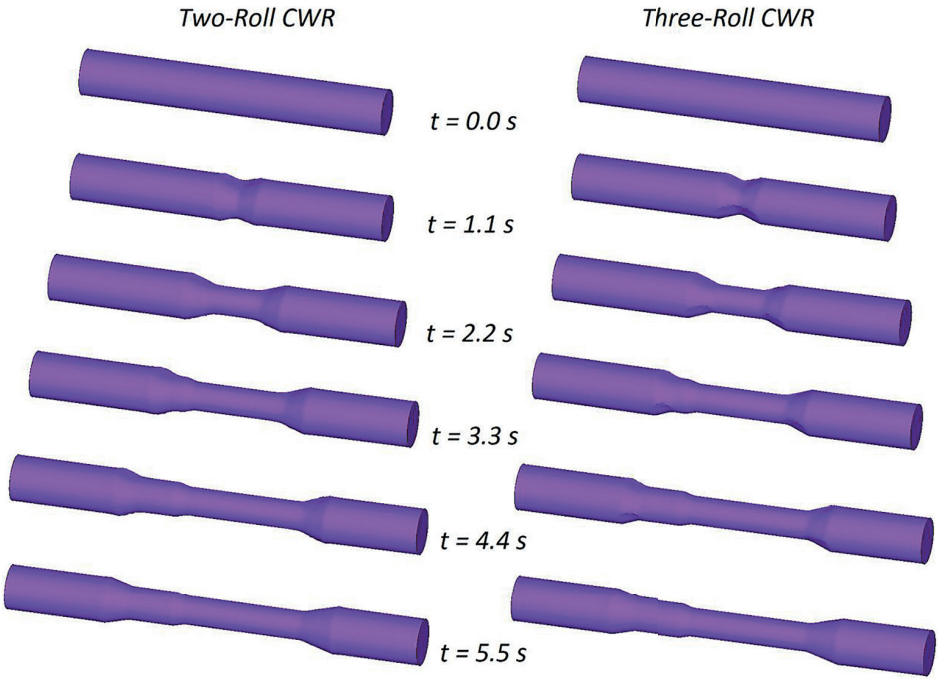

Fig. 6. Numerically modelled changes in the shape of the workpiece during the CWR processes under analysis

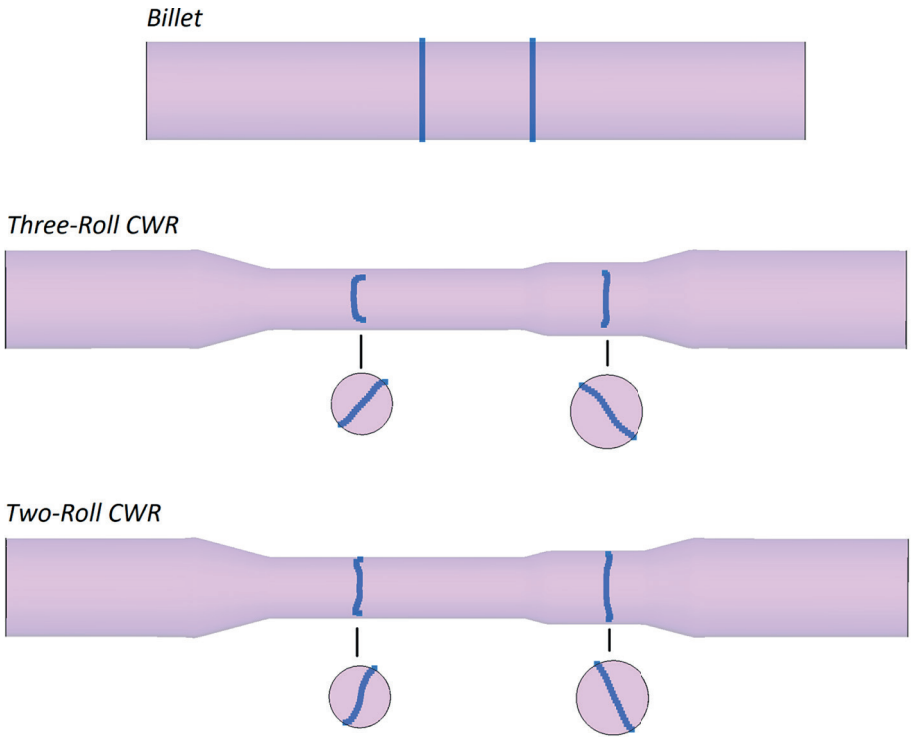

Fig. 7. Effect of the analysed CWR methods on material flow in the workpiece

shape of the workpiece. This shape was determined by the trajectory of a point that was initially located on the billet circumference, as shown in Figures 8 and 9 for CWR conducted with reduction ratios of $\delta = 1.142$ and $\delta = 1.6$, respectively. In three-roll CWR, the cross section in the transient phase, i.e. until the ultimate circular profile is achieved, assumes the shape of a triangle. In two-roll CWR, the shape is more oval. It is worth highlighting the fact that the final circular profile is achieved much faster in three-roll CWR (due to fewer revolutions of the workpiece during the forming process) than in two-roll CWR.

Material temperature

The CWR process for manufacturing a stepped shaft takes about 5.5 sec. For this reason, it is important to examine changes in material temperature. Figure 10 shows the distribution of the temperature in a shaft rolled with the use of two and three rolls, for the side view and longitudinal (axial) section. It can be observed that the temperature of the shaft rolled with the use of three rolls is lower in these regions. It seems that this results from increased contact between the rolls and the workpiece; also, the workpiece rotation rate is lower (due to the smaller diameter of the roll), which facilitates heat transfer. It must be stressed that for this CWR process, the temperature in the central region of the workpiece is relatively constant and within the recommended hot-working temperature range.

More information about temperature variations in CWR can be obtained by analysing plots in Figs. 11 and 12. The plots illustrate the changes in the temperature at six points located in a radial manner (with a spacing of every $0.2r_0$). Point 1 was initially located on the surface and point 6 along the axis of the workpiece. For both CWR processes, the greatest drops and variations in temperature can be observed on the surface of the workpiece, which results from a cyclic contact between the workpiece and the much colder tools. The temperature increases in the centre of the workpiece, with the greatest increase observed at point 1. This increase results from the exchange of deformation work into heat. A comparison of the temperatures T shown in Figs. 11 and 12 confirms that higher temperature drops occur in the three-roll CWR process. This effect can be reduced by increasing the rotational speed of the rolls, and, consequently, it would lead to a shorter forming time.

Stress and strain

The state of stress can be defined with stress invariants p, q, r described by the following equations:

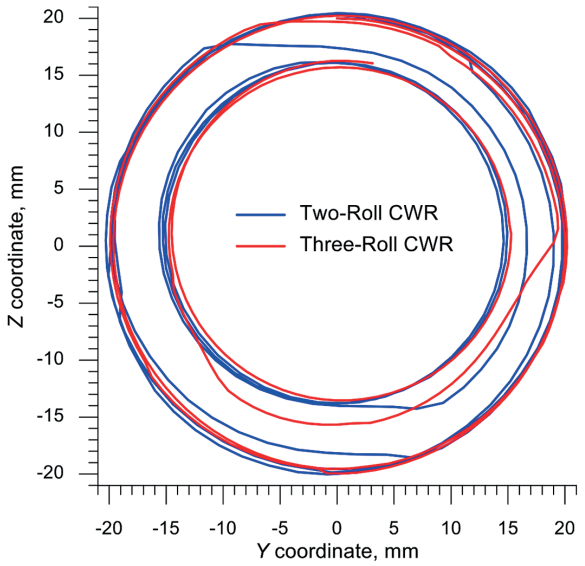

Fig. 8. Trajectory of a point describing the cross-sectional profile of a step rolled on the shaft, for two- and three-roll CWR conducted with $\delta = 1.143$

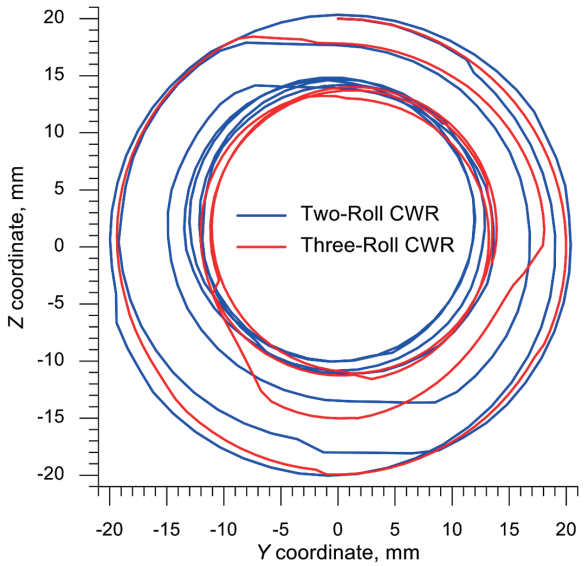

Fig. 9. Trajectory of a point describing the cross-sectional profile of a step rolled on the shaft, for two- and three-roll CWR conducted with $\delta = 1.6$

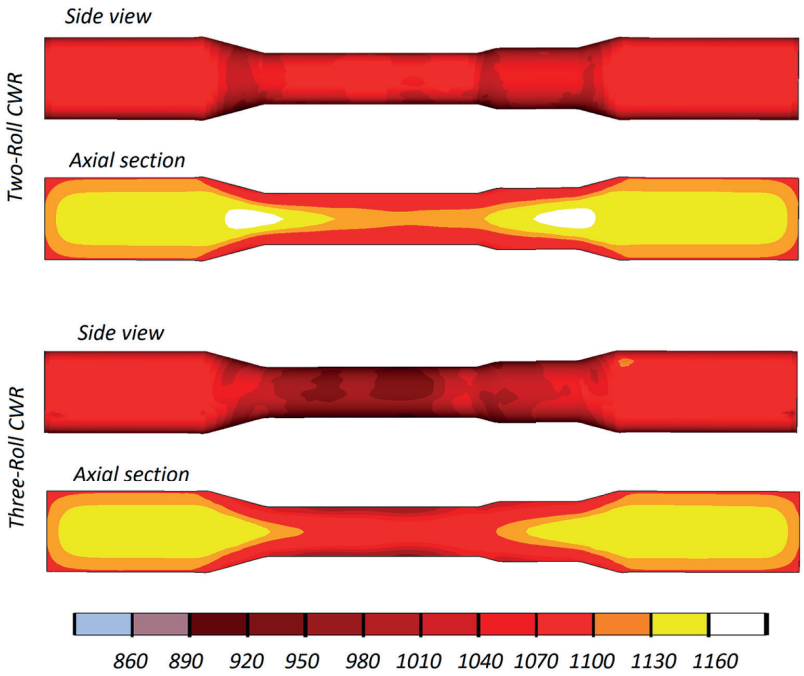

Fig. 10. Distribution of temperature (in °C) in the workpiece

$$p = -\sigma_m = -\frac{1}{3}(\sigma_1 + \sigma_2 + \sigma_3) \tag{1}$$

$$q = \sigma_i = \sqrt{\frac{1}{2}[(\sigma_1 - \sigma_2)^2 + (\sigma_2 - \sigma_3)^2 + (\sigma_1 - \sigma_3)^2]} \tag{2}$$

$$r = \left[\frac{27}{2}(\sigma_1 - \sigma_m)(\sigma_2 - \sigma_m)(\sigma_3 - \sigma_m)\right]^{\frac{1}{3}} \tag{3}$$

where: σ_1, σ_2, σ_3 – principal stresses, σ_m – the mean stress, σ_i – the effective or equivalent stress.

The state of stress is often defined with the stress triaxiality η and the Lode angle parameter θ, both of which are described by means of

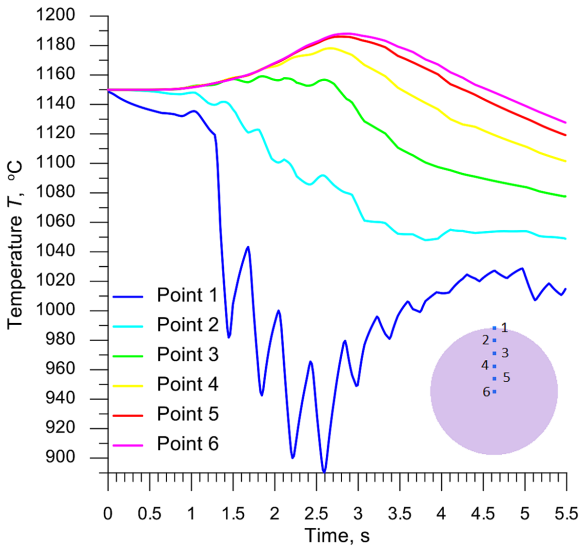

Fig. 11. Temperature T at measuring points in the workpiece, for two-roll CWR conducted with δ=1.6

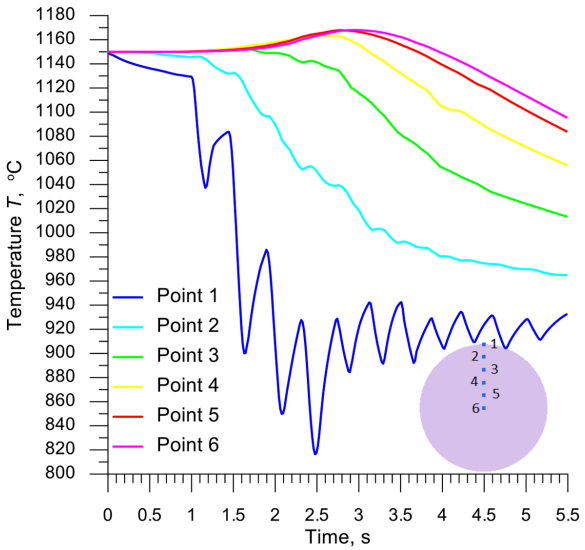

Fig. 12. Temperature T at measuring points in the workpiece, for three-roll CWR conducted with δ=1.6

the stress invariants according to the following equations:

$$\eta = \frac{-p}{q} = \frac{\sigma_m}{\sigma_i} \tag{4}$$

$$\theta = 1 - \frac{2}{\pi}\arccos\left[\left(\frac{r}{q}\right)^3\right] \tag{5}$$

The parameters η and θ change during CWR. Therefore, for the purpose of comparing these parameters in two- and three-roll CWR processes, their mean values were calculated according to the following equations:

$$\eta_{av} = \frac{1}{\varepsilon}\int_0^{\varepsilon} \eta \, d\varepsilon \tag{6}$$

$$\theta_{av} = \frac{1}{\varepsilon}\int_0^{\varepsilon} \theta \, d\varepsilon \tag{7}$$

where: ε – the equivalent plastic strain.

In Figure 13 the $\eta\theta$ coordinates are used to compare the stresses at six points located at different distances from the axis of the workpiece, with the initial distance set to $0.2r_0$ (with point 1 located on the surface and point 6 along the workpiece axis). An analysis of the data in the figure reveals that the stresses in the surface layer are relatively similar for both CWR processes. For this region, the stress triaxiality is η<0, which means that material cohesion loss might occur as a result of shear. The number of the rolls has a significant impact on the stress state in the axial zone of the workpiece. Differences can primarily be observed with respect to the Lode angle parameter θ, as the stress triaxiality is at a similar level of 0<η<0.2 (for this range of η, material cohesion loss can be caused by shear as well as void nucleation, growth and coalescence). The Lode angle parameter in two-roll CWR has a value of $\theta \approx -0.65$, whereas in three-roll CWR it is about 0.95 (these values refer to the points located along the axis of the workpiece). Also, it can be observed that the change in the reduction ratio δ has no significant effect on the stress state in the workpiece. According to previous studies [37, 38], an increase in the absolute value of the θ parameter leads to an increased value of the critical strain ε_f causing material fracture. It can therefore be claimed that the stress state in the axial zone of the workpiece in two-roll CWR is more conducive to material cracking than that observed in three-roll CWR.

Figure 14 shows the distributions of strains in a stepped shaft produced by two- and three-roll CWR. Considerably higher strains can be observed in the part rolled with the use of two tools, which means that in this process there was a more rapid material flow in the tangential (circumferential) direction, leading to the increased redundant strains. For both CWR processes, the strains are distributed in layers (ring-shaped) and achieve the highest values in the surface layer due

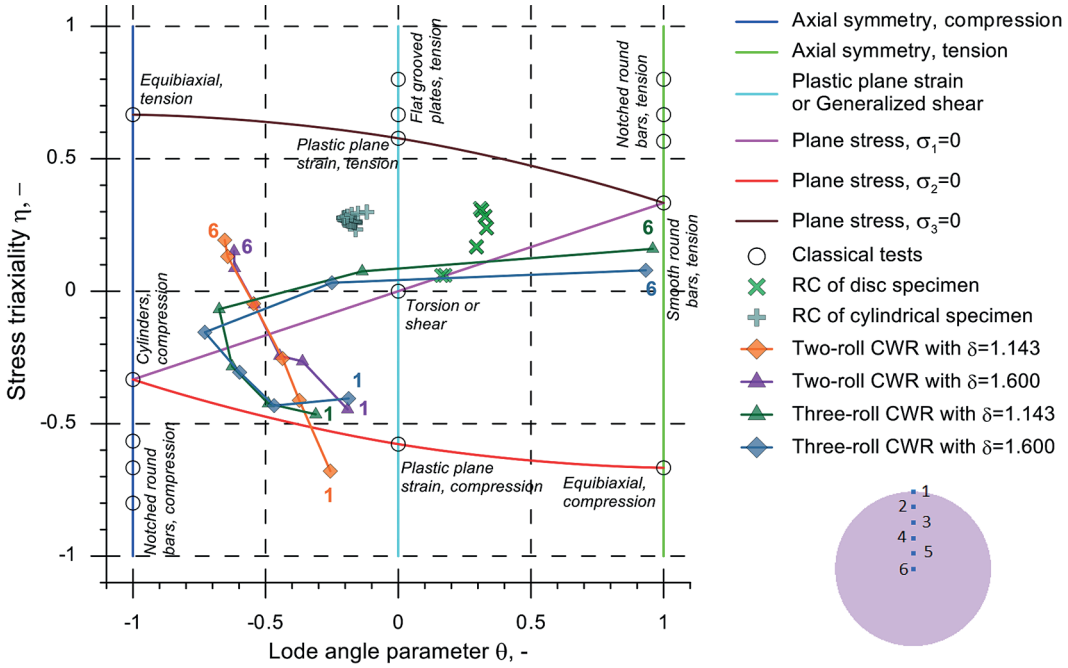

Fig. 13. Comparison of stresses in parts formed by CWR

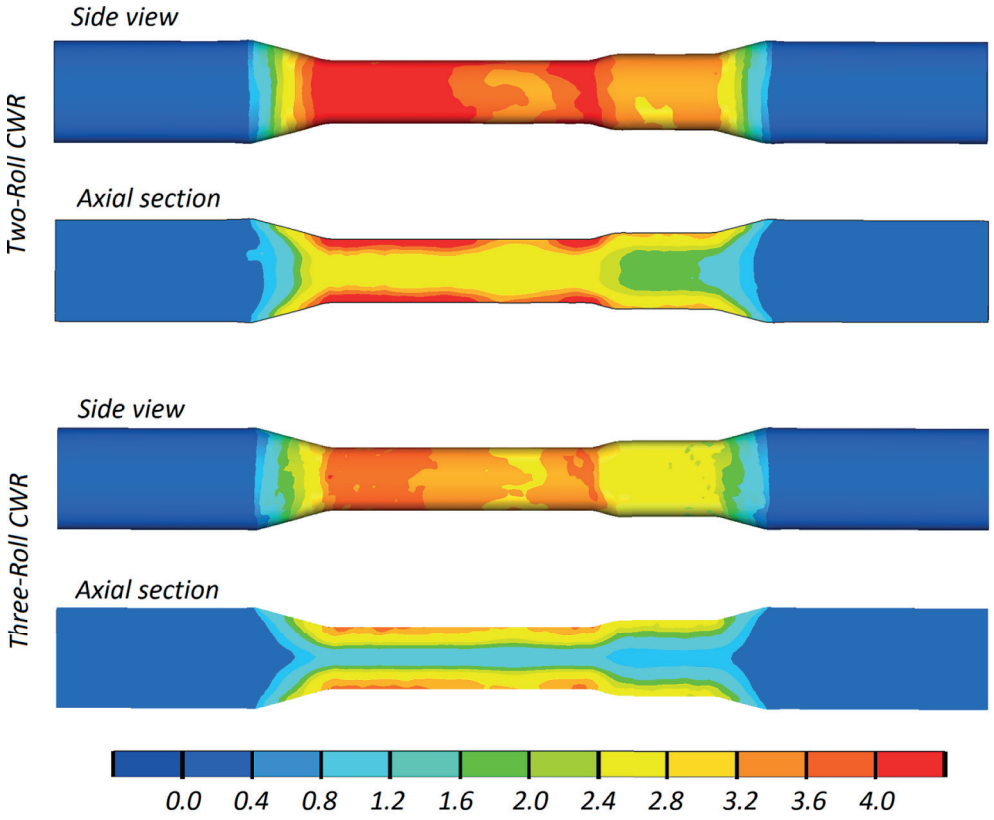

Fig. 14. Effective strains in the workpiece

to the presence of friction forces that make the workpiece rotate.

Figures 15 and 16 show the changes in the effective strain at the measuring points in the cross section of the workpiece during two- and three-roll CWR, respectively. For both processes, the pattern of changes is identical. The strains increase during cross-sectional reduction, and their values remain practically unchanged during sizing once the final circular shape has been achieved. A comparison of the effective strain values demonstrates that the strains in the shaft rolled with three rolls

are lower (by about 2.8 times in the axis and by about 1.2 times on the surface) than those in the part rolled using two rolls. This strain distribution indicates that parts produced by three-roll CWR have lower susceptibility to internal crack formation.

Failure modes in CWR

The stability of CWR can be undermined by the following failure modes: workpiece slipping which leads to halting workpiece rotation, workpiece core necking (rupture), as well as internal crack formation.

Workpiece slipping

Workpiece slipping leading to halting workpiece rotation occurs when the sum of the moments of forces causing rotation is smaller than the sum of the moments of forces preventing this rotation. The susceptibility to slipping in CWR can be estimated by analysing the rolling radius r_t [2] which is expressed with the equation:

$$r_t = \frac{a}{\frac{\omega_w}{\omega_R} + 1} \tag{8}$$

where: a – the distance between the axes of the rolls and the workpiece, ω_w – the angular velocity of the workpiece, ω_R – the angular velocity of the roll.

Equation 8 demonstrates that any decrease in the rotational speed of the workpiece (while maintaining a constant value of ω_R) leads to an increase in the rolling radius r_t. For the extreme case, when the workpiece stops rotating, the rolling radius is equal to the distance a.

Figure 17 shows the rolling radius for the two analysed CWR processes. It can be observed that the rolling radius r_t is lower and has a more stable value in three-roll CWR. The mean value of r_t calculated for the time interval $t\epsilon(0.5s; 5s)$ is 20.95 mm in two-roll CWR and 19.07 mm in three-roll CWR. The lower value of r_t in three-roll CWR means that this process is less susceptible to the occurrence of workpiece slipping that would disturb the forming process stability.

Core necking (rupture)

Core necking occurs when tensile stresses acting in the axial direction reach the flow stress value in the material. This leads to the formation of a neck that resembles the one typical of tension. In the extreme case, the neck can be ruptured.

To examine the susceptibility to neck formation in the two analysed CWR processes, a ratio of axial stress σ_x to flow stress σ_F was calculated at the six measuring points in the workpiece. Obtained results of the σ_x/σ_F ratio are shown in Figs. 18 and 19 for two- and three-roll CWR, respectively.

An analysis of the data in the figures demonstrates that in two-roll CWR, the condition required for initiating the necking of a rolled step

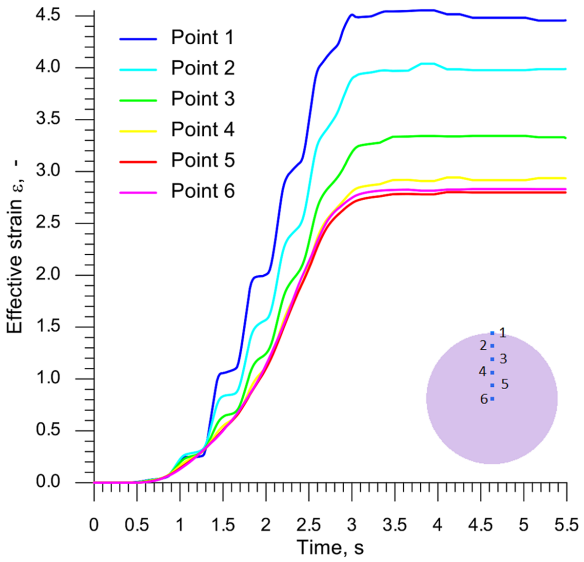

Fig. 15. Effective strain ε at measuring points in the workpiece, for two-roll CWR conducted with $\delta = 1.6$

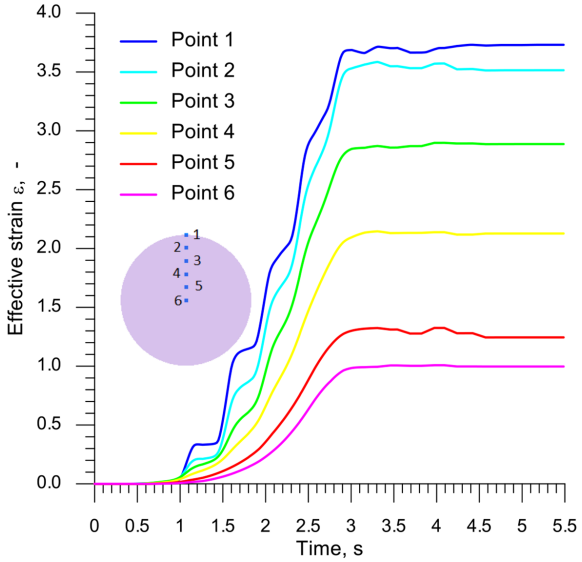

Fig. 16. Effective strain ε at measuring points in the workpiece, for three-roll CWR conducted with $\delta = 1.6$

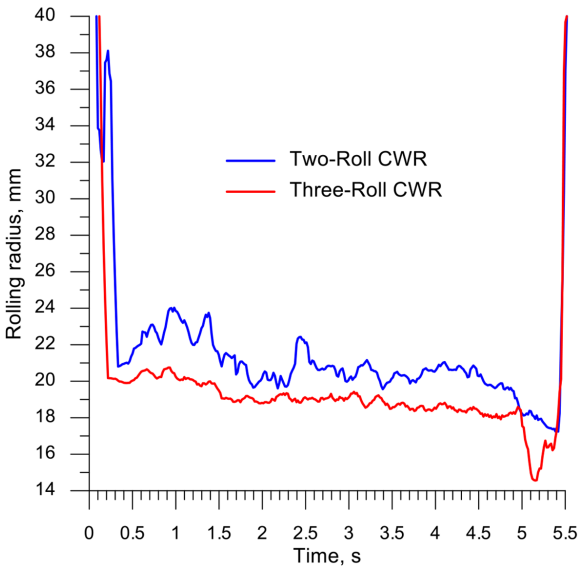

Fig. 17. Rolling radii in the CWR processes under analysis

$$\frac{\sigma_x}{\sigma_F} \geq 1 \tag{9}$$

is not satisfied at any point in the cross section of the workpiece. In contrast, for three-roll CWR, the above condition is satisfied toward the end of the rolling process (t>3.8 s) at points 5 and 6 located in the axial zone of the workpiece. At the same time, however, in the surface zone (points 1 and 2) the stresses σ_x are negative, which proves that the axial flow of the material is impeded (by the impact of friction forces) and thus neck formation is prevented. Nevertheless, the numerical results demonstrate that the risk of neck formation (rupture) is greater in three-roll CWR than in two-roll CWR. This undoubtedly results from the use of higher values of the spreading angle β.

Internal cracking

Ductile fracture that may occur in the workpiece during CWR can be predicted with so-called failure criteria. Among the many failure criteria [3, 39], the most popular is the normalised Cockcroft-Latham criterion [40]. According to this criterion, material fracture is described by the damage function f_{CL} expressed as a ratio of maximum principal stress to effective stress σ_i as follows:

$$f_{CL} = \int_0^{\varepsilon} \frac{\sigma_1}{\sigma_i} d\varepsilon. \tag{10}$$

Material fracture occurs when the damage function f_{CL} reaches its critical value C, this value being calculated via so-called calibration tests.

Figure 20 shows the damage function f_{CL} in stepped shafts produced by two- and three-roll CWR. It can clearly be observed that the risk of internal crack formation is greater in the two-roll CWR process, which is proved by the fact that considerably higher f_{CL} values are located in the axial zone of the workpiece.

Changes in the damage function f_{CL} at the six measuring points are shown in Figures 21 (two-roll CWR) and 22 (three-roll CWR). For two-roll

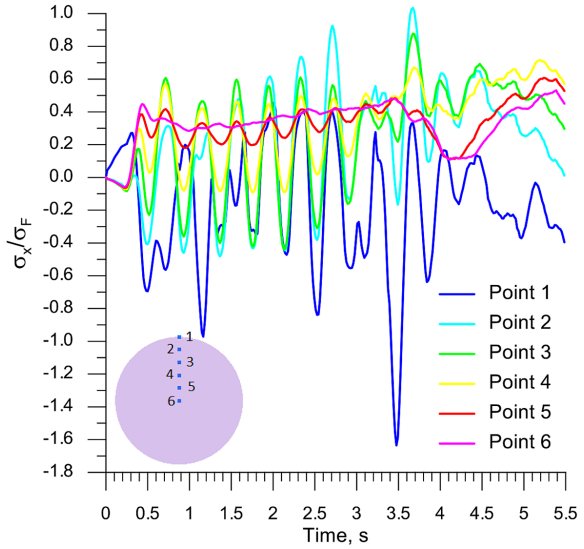

Fig. 18. Ratio of axial stress σ_x to flow stress σ_F at measuring points in the workpiece, for two-roll CWR conducted with δ=1.6

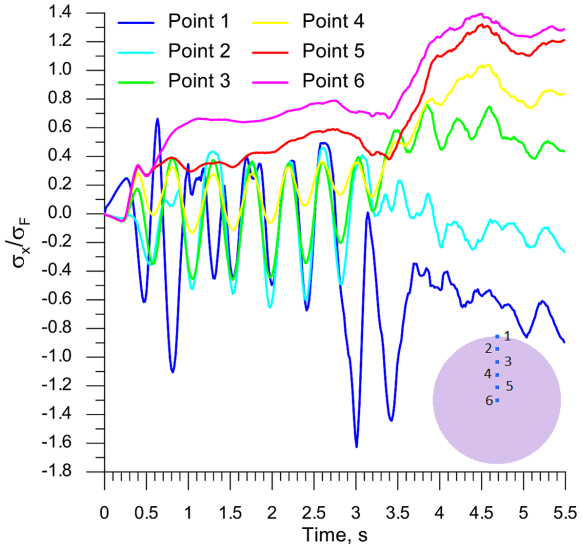

Fig. 19. Ratio of axial stress σ_x to flow stress σ_F at measuring points in the workpiece, for three-roll CWR conducted with δ=1.6

CWR, the highest values of f_{CL} ($f_{CL} \approx 1.6$) are located along the axis of the workpiece. Regarding the three-roll CWR process, the highest f_{CL} values of about 0.9 are located on the surface of the rolled step. In the axial zone of the workpiece, the damage function is lower and has a value of $f_{CL} \approx 0.7$, which amounts to 44% of the value obtained for the CWR process conducted with the use of two rolls. It can therefore be claimed that the three-roll CWR process is less susceptible to internal crack formation in the workpiece.

Load and energy parameters

Radial load affects rolling process accuracy because it causes mill stretch, which – in turn – changes the diameter of a step formed on the shaft. Figure 23 shows the distribution of this load for the two analysed CWR processes. It can be observed that the maximum radial load in two-roll CWR is 98.7 kN, and the mean value of this load determined for the entre forming cycle is equal to 71.85 kN. For the three-roll CWR process, these values are, respectively, 92.0 kN and 63.53 kN (which amounts to 93.2% of the maximum radial load and to 88.4% of the mean radial load in two-roll CWR). It can therefore be claimed that the three-roll CWR process is more advantageous due to lower mill stretch.

Figure 24 shows the distribution of torques for the analysed CWR processes. Although the torques are very similar in terms of quality, they significantly differ in terms of their values. Specifically, the maximum torque is 5938.8 Nm for two-roll CWR and 3001.1 Nm for three-roll CWR. Based on the obtained maximum torque values, it can be claimed that the engine power required for driving a single roll in a two-roll mill must be twice as high as that in a three-roll machine. Taking into account the number of engines, it can be stated that the power demand of a two-roll mill is 4/3 of that for a three-roll mill.

Using the data given in Figure 24 one can calculate the mean torque for the entire forming cycle. This torque value is 4048.8 Nm and 1984.7 Nm for two-roll CWR and three-roll CWR, respectively. Considering the mean torque values and the number of the rolls, it is possible to determine the value of energy that is required for forming a shaft, this value being 47.04 kJ for two-roll CWR and 34.59 kJ for three-roll CWR. This means that the work required for forming a shaft in two-roll CWR is 35% higher than that in three-roll CWR.

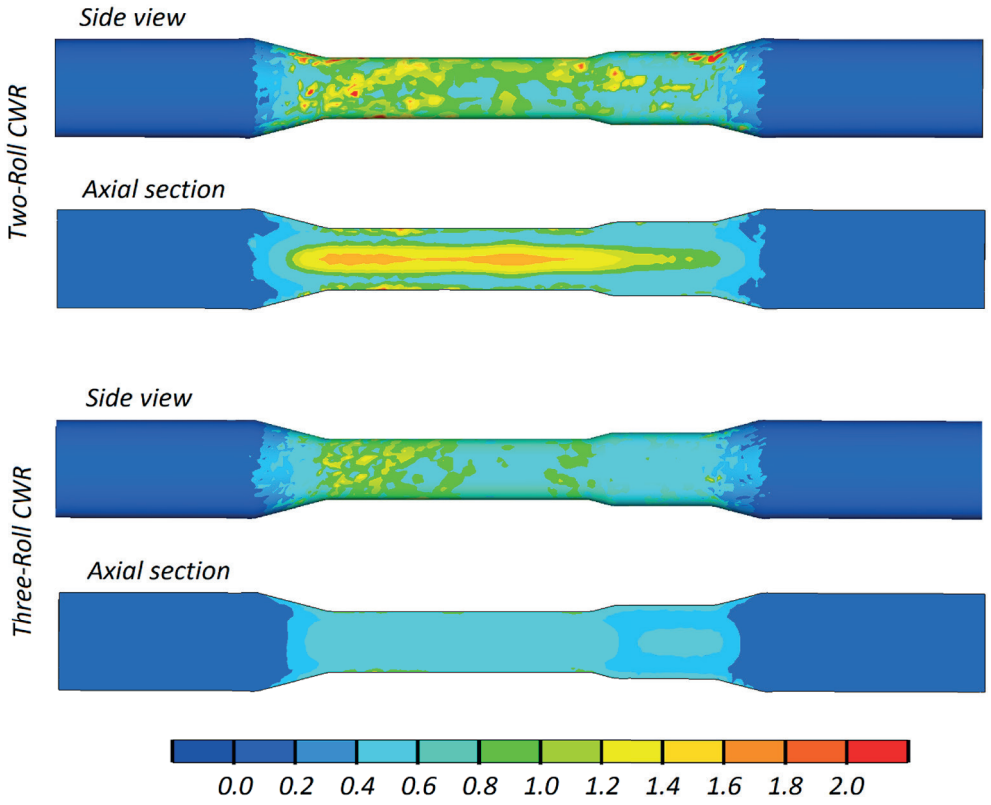

Fig. 20. Distribution of the damage function (calculated according to the Cockcroft-Latham criterion) in the workpiece

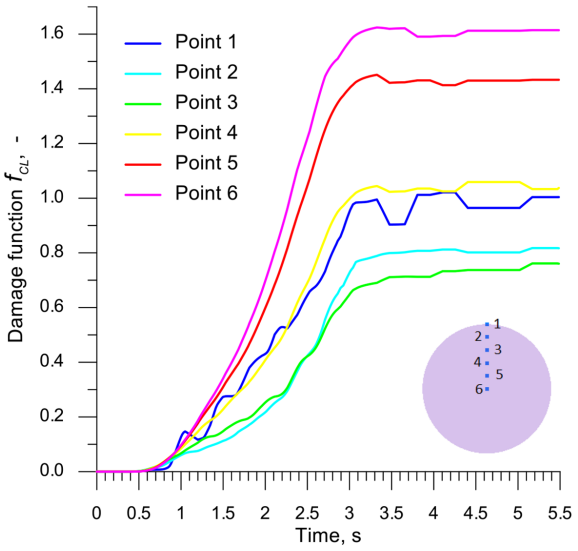

Fig. 21. Distribution of the damage function f_{CL} (calculated according to the Cockcroft-Latham criterion) at measuring points in the workpiece, for two-roll CWR conducted with $\delta = 1.6$

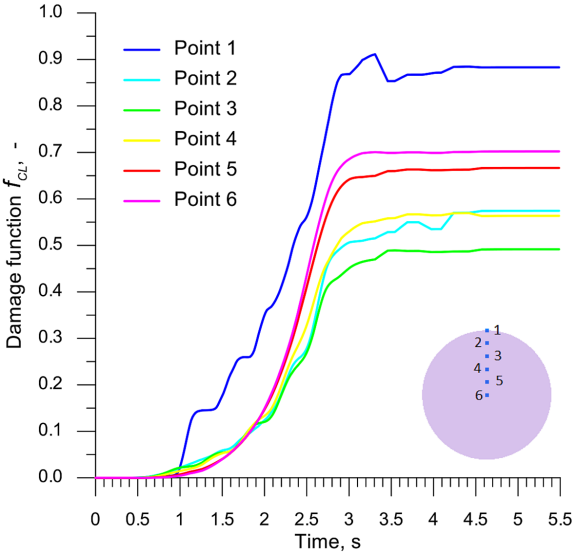

Fig. 22. Distribution of the damage function f_{CL} (calculated according to the Cockcroft-Latham criterion) at measuring points in the workpiece, for three-roll CWR conducted with $\delta = 1.6$

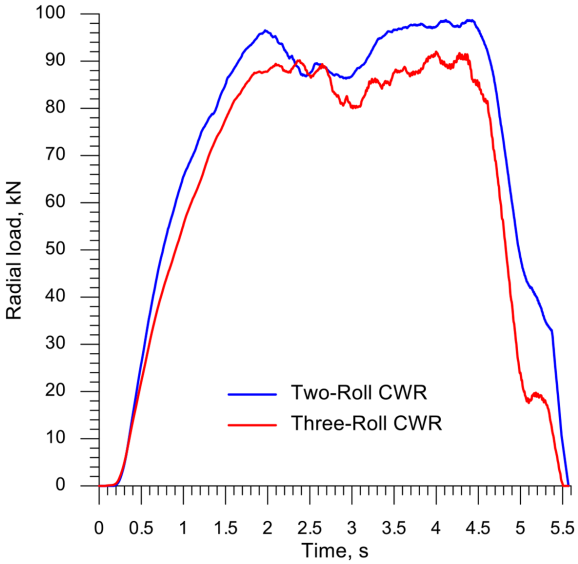

Fig. 23. Radial loads in the CWR processes under analysis

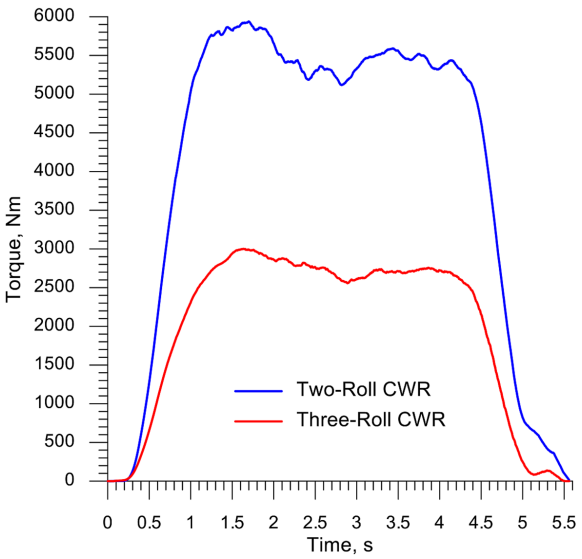

Fig. 24. Torques in the CWR processes under analysis

CONCLUSIONS

The results of a comparative numerical analysis between the three- and two-roll CWR processes lead to the following conclusions. Compared to the widely used two-roll CWR process, CWR conducted with three rolls is characterized by:

- faster achievement of the desired circular profile of a step formed on the shaft;
- higher drops in material temperature due to increased contact between the rolls and the workpiece as well as a lower rotational speed of the workpiece;
- the stress state that requires higher strains in the axial zone of the workpiece to induce internal crack formation;
- considerably lower strains resulting from a constrained metal flow in the tangential direction;
- reduced susceptibility to slipping that would prevent workpiece rotation;
- higher risk of core necking (rupture) in the workpiece as a result of using higher values of the spreading angle β;

- lower probability of internal crack formation in the workpiece;
- lower radial loads and thus reduced mill stretch;
- lower energy consumption.

The above conclusions clearly demonstrate that further studies should be conducted on three-roll CWR. For this reason, a specialist test stand for this forming process will be constructed at the Lublin University of Technology. Results obtained from these tests will subsequently be reported in scientific publications.

REFERENCES

1. Gronostajski Z., Pater Z., Madej L., Gontarz A., Lisiecki L., Łukaszek-Sołek A., et al. Recent development trends in metal forming. Archives of Civil and Mechanical Engineering. 2019; 19(3): 898-941.
2. Pater Z. Cross-Wedge Rolling, Comprehensive Materials Processing; Button ST, Ed.; Elsevier Ltd., 2014; 3: 211–279.
3. Pater Z., Tomczak J., Bulzak T., Wójcik Ł., Walczuk P. Assessment of ductile criteria with respect to their application in the modeling of cross wedge rolling. Journal of Materials Processing Technology. 2020; 278: e116501.
4. Slick E.E. Manufacture of axles. US Patent no 470,354 (1892).
5. Schneider F.R. Rolls for the manufacture of axles. US Patent no 679,998 (1901).
6. Wurster A.L. Roll press. US Patent 1,493,836 (1924).
7. Brown T.E. Rotary forging machine. US Patent no 2,342,917 (1944).
8. Wilson H.M. Machine for deforming billets. US Patent no 2,686,442 (1954).
9. Rogers S.E. The impact of drop forging research. Metal Forming. 1970; December: 356–361, 367.
10. Thomas A. Transverse rolling of preforms for drop forging. Proc. 1st Int. Conf. on Rotary Metalworking Processes, 20–22 November, 1979, London, UK, 147–156.
11. Danno A., Tanaka T. Characteristics of billet deformation in 3-roll wedge rolling of axisymmetric stepped shafts. In: Proc. 3rd Int. Conf. on Rotary Metalworking Processes; 8–10 September 1984; Kyoto, Japan, 321–332.
12. Pater Z., Bartnicki J., Gontarz A., Weroński W.W. Numerical Modelling of Cross-Wedge Rolling of Hollowed Shafts. AIP Conference Proceedings. 2004; 712: 672–677.
13. Bartnicki J., Pater Z. Numerical simulation of three-rolls cross wedge rolling of hollowed shaft. Journal of Materials Processing Technology. 2005; 164–165: 1154–1159.
14. Pater Z. Finite element analysis of cross wedge rolling. Journal of Materials Processing Technology. 2006; 173: 201–208.
15. Qiu P., Xiao H., Li M. Effect of Non-uniform Temperature Field on Piece Rolled by Three-roll Cross Wedge Rolling. Advanced Mechanics and Materials. 2009; 16–19: 456–461.
16. Pater Z., Lis K., Walczuk-Gągała P. Numerical Analysis of the Cross-Wedge of a Hollow Rail Axle. Advances in Science and Technology Research Journal. 2020; 14(1): 145–153.
17. Pater Z., Gontarz A., Weroński W. Cross-wedge rolling by means of one flat Wedge and two shaped Rolls. Journal of Materials Processing Technology. 2006; 177: 550–554.
18. Tofil A., Tomczak J., Bulzak T., Pater Z., Buczaj M., Sumorek A. A Rotary Compression Process for Producing Hollow Gear Shafts. Materials 2020; 13: e5718.
19. Tomczak J., Pater Z., Bulzak T. The influence of hollow billet thickness in rotary compression. The International Journal of Advanced Manufacturing Technology. 2016; 82: 1281–1291.
20. Pater Z., Tomczak J., Bulzak T., Wójcik Ł. Conception of a Three Roll Cross Rolling Process of Hollow Rail Axles. ISIJ International. 2021; 61: 895–901.
21. Pater Z., Wójcik Ł., Walczuk P. Comparative Analysis of Tube Piercing Processes in the Two-Roll and Three-Roll Mills. Advances in Science and Technology Research Journal. 2019; 13(1): 37–45.
22. Skripalenko M.M., Romantsev B.A., Galkin S.P., Kaputkina L.M., Skripalenko M.N., Danilin A.V., et al. Forming Features at Screw Rolling of Austenic Stainless-Steel Billets. Journal of Materials Engineering and Performance. 2020; 29: 3889–3894.
23. Yamane K., Shimoda K., Kuroda K., Kajikawa S., Kuboki T. A new ductile fracture criterion for skew rolling and its application to evaluate the effect of number rolls. Journal of Materials Processing Technology. 2021; 291: e116989.
24. Pater Z., Tomczak J., Bulzak T., Wójcik Ł., Skripalenko M.M. Prediction of ductile fracture in skew rolling processes. International Journal of Machine Tools and Manufacture. 2021; 163: e103706.
25. Pater Z., Tomczak J., Bulzak T. Numerical analysis of the skew rolling process for rail axles. Archives of Metallurgy and Materials. 2015; 60(1): 415–418.

26. Xu C., Shu X.D. Influence of process parameters on the forming mechanics parameters of the three-roll skew rolling forming of the railway hollow shaft with 1:5. Metalurgija. 2018; 57(3): 153–156.
27. Bartnicki J., Xia Y., Shu X. The chosen aspects of skew rolling of hollow stepped shafts. Materials. 2021; 14: e764.
28. Cao Q., Hua L., Qian D. Finite element analysis of deformation characteristics in cold helical rolling of bearing steel-balls. Journal of Central South University. 2015; 22: 1175–1183.
29. Lis K., Wójcik Ł., Pater Z. Numerical analysis of a skew rolling process for producing a crankshaft preform. Open Engineering. 2016; 6: 581–4.
30. Huang H., Chen X., Fan B., Jin Y., Shu X. Initial billet temperature influence and location investigation on tool wear in cross wedge rolling. The International Journal of Advanced Manufacturing Technology. 2015; 79: 1545–56.
31. Tofil A., Tomczak J., Bulzak T. Numerical and experimental study on producing aluminum alloy 6061 shafts by cross wedge rolling using a universal rolling mill. Archives of Metallurgy and Materials. 2015; 60(2): 801–807.
32. Lu L., Wang Z., Wang F., Zhu G., Zhang X. Simulation of tube forming process in Mannesmann mill. Journal of Shanghai Jiaotong University (Science). 2011; 16(3): 281–285.
33. Li Z., Shu X. Involute Curve Roller Trace Design and Optimization in Multipass Conventional Spinning Based on the Forming Clearance Compensation. ASME Journal of Manufacturing Science and Engineering. 2019; 141(9): e091007.
34. Berti G.A., Quagliato L., Monti M. Set-up of radial–axial ring-rolling process: Process worksheet and ring geometry expansion prediction. International Journal of Mechanical Sciences. 2015; 99: 58–71.
35. Quagliato L., Berti G.A. Mathematical definition of the 3D strain field of the ring in the radial-axial ring rolling process. International Journal of Mechanical Sciences. 2016; 115–116: 746–759.
36. Groche P., Kramer P. Numerical investigation of the influence of frictional conditions in thread rolling operations with flat dies. International Journal of Material Forming. 2018; 11: 687–703.
37. Bai Y., Teng X., Wierzbicki T. On the application of stress triaxiality formula for plane strain fracture testing. Journal of Engineering Materials and Technology, Transactions of the ASME. 2009; 131(2): e021002.
38. Bulzak T., Pater Z., Tomczak J., Wójcik Ł., Murillo-Marrodán A. Internal crack formation in cross wedge rolling: Fundamentals and rolling methods. Journal of Materials Processing Technology. 2022; 307: e117681.
39. Pater Z., Tomczak J., Bulzak T., Bartnicki J., Tofil A. Prediction of Crack Formation for Cross Wedge Rolling of Harrow Tooth Preform. Materials. 2019; 12: e2287.
40. Cockcroft M.G., Latham D.J. Ductility and the workability of metals. Journal of the Institute of Metals. 1968; 96: 33–39